Role of OH radicals in the formation of oxygen molecules following vacuum ultraviolet photodissociation of amorphous solid water

Tetsuya Hama, Masaaki Yokoyama, Akihiro Yabushita, and Masahiro Kawasaki

Citation: J. Chem. Phys. **133**, 104504 (2010); doi: 10.1063/1.3474999
View online: http://dx.doi.org/10.1063/1.3474999
View Table of Contents: http://jcp.aip.org/resource/1/JCPSA6/v133/i10
Published by the American Institute of Physics.

Role of OH radicals in the formation of oxygen molecules following vacuum ultraviolet photodissociation of amorphous solid water

Tetsuya Hama,[1,2,a)] Masaaki Yokoyama,[2] Akihiro Yabushita,[2] and Masahiro Kawasaki[2,b)]
[1]*Institute of Low Temperature Science, Hokkaido University, Sapporo 060-0819, Japan*
[2]*Department of Molecular Engineering, Kyoto University, Kyoto 615-8510, Japan*

(Received 3 March 2010; accepted 14 July 2010; published online 13 September 2010)

Photodesorption of $O_2(X\ ^3\Sigma_g^-)$ and $O_2(a\ ^1\Delta_g)$ from amorphous solid water at 90 K has been studied following photoexcitation within the first absorption band at 157 nm. Time-of-flight and rotational spectra of O_2 reveal the translational and internal energy distributions, from which production mechanisms are deduced. Exothermic and endothermic reactions of $OH+O(^3P)$ are proposed as plausible formation mechanisms for $O_2(X\ ^3\Sigma_g^-$ and $a\ ^1\Delta_g)$. To examine the contribution of the $O(^3P)+O(^3P)$ recombination reaction to the O_2 formation following 157 nm photolysis of amorphous solid water, O_2 products following 193 nm photodissociation of SO_2 adsorbed on amorphous solid water were also investigated. © *2010 American Institute of Physics*.
[doi:10.1063/1.3474999]

I. INTRODUCTION

The effect of radiation on water ice has intrigued many scientists in the fields of interstellar chemistry and planetary ice science as well as reaction dynamics since water is the predominant component of interstellar icy grain mantles in dense molecular clouds and small solar system bodies such as comets.[1,2] Oxygen molecule is known to be a product when water ice is irradiated with photons, electrons, or with energetic ions.[3–6] Westley *et al.*[7,8] observed desorption of H_2, O_2, and H_2O by a quadrupole mass spectrometer (QMS) during vacuum ultraviolet (VUV) irradiation of water ice at 35–100 K with mainly Lyman-α photons ($\lambda \cong 121$ nm). Öberg *et al.*[9] used a VUV lamp (118 nm $\leq \lambda \leq$ 177 nm) to irradiate water ice at 18–100 K, and detected OH, H_2, O_2, and H_2O as desorbing species by QMS. These experimental studies indicate that VUV photodissociation of amorphous solid water (ASW) leads to secondary reactions that result in molecular oxygen formation on or in ASW.

Various primary processes are energetically possible following photoexcitation of water ice at $\lambda \leq 130$ nm,[10–12] whereas photodissociation of H_2O in the first absorption band of water ice (130–165 nm) involves mainly two primary processes,[10,13,14]

$$H_2O + h\nu \rightarrow H + OH, \quad (1)$$

$$H_2O + h\nu \rightarrow H_2 + O(^1D). \quad (2)$$

Measurements of the translational and internal energy distributions of the photoproducts generated from photodissociation of ASW allow the assessment of possible secondary reactions on/in ASW from reaction dynamics point of view. The translational and internal energy distributions of $OH(v=0,1)$ radicals and $O(^1D$ and $^3P)$ atoms were previously measured following 157 nm photodissociation of ASW.[15–17] For the $O(^3P)$ production, two different formation mechanisms were proposed: the exothermic recombination reaction of OH and the photodissociation of OH on the ASW surface,[17]

$$OH + OH \rightarrow H_2O + O(^3P), \quad \Delta H = -67 \text{ kJ mol}^{-1}, \quad (3)$$

$$OH(\text{ads}) + h\nu \rightarrow H + O(^3P). \quad (4)$$

Thermodynamic data are calculated using solid phase data for the condensed or adsorbed species ("ads") and the gas phase data for other species.[18–20] From the fact that $OH(v=0$ and 1) and $O(^3P)$ are formed with large excess energy via reactions (1), (3), and (4),[15,17] $O_2(X\ ^3\Sigma_g^-)$ and $O_2(a\ ^1\Delta_g)$ can be produced via subsequent reactions (5) and (6) in the 157 nm photolysis of ASW,

$$OH + O(^3P) \rightarrow O_2(X\ ^3\Sigma_g^-) + H, \quad \Delta H = -68 \text{ kJ mol}^{-1}, \quad (5)$$

$$OH + O(^3P) \rightarrow O_2(a\ ^1\Delta_g) + H, \quad \Delta H = 26 \text{ kJ mol}^{-1}. \quad (6)$$

Reaction (5) is a barrierless process in the gas phase.[21] $OH(v=1)$ has a sufficient vibration energy of 43 kJ mol^{-1} to proceed in reaction (6).[22] In fact, Lunt *et al.*[23] observed the formation of $O_2(a\ ^1\Delta_g)$ via the reaction of $O(^3P)$ and vibrationally excited $OH(v \geq 1)$ in the gas phase by monitoring the near-infrared emission at 1.27 μm from the product $O_2(a\ ^1\Delta_g)$.

In the present work, we have investigated the kinetic and internal energy distributions of $O_2(X\ ^3\Sigma_g^-, v=0)$ and $O_2(a\ ^1\Delta_g, v=0)$ following 157 nm photodissociation of ASW at 90 K using the resonance-enhanced multiphoton-ionization (REMPI) method. H_2O_2 photolysis experiments have also been performed at 157 nm to elucidate the role of OH in the O_2 formation. In addition, we have also studied desorption of O_2 following 193 nm photolysis of SO_2 adsorbed on ASW to measure the kinetic and internal energy

a)Present address: Institute of Low Temperature Science, Hokkaido University, Sapporo 060–0819, Japan.
b)Author to whom correspondence should be addressed. Electronic mail: kawasaki@moleng.kyoto-u.ac.jp. FAX: +81-75-383-2572.

TABLE I. Spectroscopic constants for the upper $d\ ^1\Pi_g$ and $C\ ^3\Pi_g$ Rydberg states, and the lower $X\ ^3\Sigma_g^-$ states of O_2. [The values of state origins for $d\ ^1\Pi_g(v'=2)$ and $C\ ^3\Pi_g(v'=3,\ 4,\ \text{and}\ 5)$ were taken from Ref. 35. The values of state origins for $X\ ^3\Sigma_g^-(v''=2\ \text{and}\ 3)$ were taken from Refs. 36 and 37.]

	State origin (cm^{-1})	Rotational constant B (cm^{-1})	Centrifugal distortion constant D (10^{-6} cm^{-1})	Reference
$C\ ^3\Pi_g(v=2)$, $F_1(\Omega=0)$	69 353	1.633	1.5	30
$C\ ^3\Pi_g(v=2)$, $F_2(\Omega=1)$	69 437	1.665	1.0	30
$C\ ^3\Pi_g(v=2)$, $F_3(\Omega=2)$	69 548	1.685	1.3	30
$d\ ^1\Pi_g(v=2)$	70 011	1.29		35
	70 142[a]	1.12[a]		
$X\ ^3\Sigma_g^-(v=1)$	1556.3	1.422	4.8402	38
$X\ ^3\Sigma_g^-(v=0)$	0	1.438	4.8390	39

[a]Second entry refers to the extra level $II\ ^1\Pi_g(v=8)$ (see Ref. 35).

distributions of O_2 formed via highly exothermic recombination reaction of two $O(^3P)$, i.e., reaction (7), which was proposed as a source for $O_2(X\ ^3\Sigma_g^-)$ formation in VUV photon and electron irradiations of ASW,[8,24]

$$O(^3P) + O(^3P) + M \rightarrow O_2\left(X\ ^3\Sigma_g^-\right) + M, \quad \Delta H\ (\text{kJ mol}^{-1}) = -498. \tag{7}$$

II. EXPERIMENTAL

A. Apparatus and preparation of ice

A photodissociation study of ASW at 90 K was carried out in an ultrahigh vacuum chamber, which was equipped with two turbomolecular pumps in tandem, a pulsed molecular beam, an excimer laser, and a dye laser. Experimental details are described elsewhere.[25] A vacuum chamber was evacuated to a base pressure of 10^{-8} Torr by turbomolecular pumps (800 and 50 L s^{-1}). ASW was prepared with the backfilling deposition of water vapor for 60 min onto an optically flat sapphire disk substrate, sputter coated with a thin polycrystalline film of Au(111) cooled by liquid nitrogen at 90 K. The exposure was typically 1500 L (1 L=1×10^{-6} Torr s). This exposure resulted in the formation of roughly 500 ML (monolayer) of H_2O on the substrate if we adopt the reported experimental conversion factor of 1 ML deposition by 3 L exposure,[26] which is sufficiently thick to neglect the possible influence of reactions at the ASW/Au substrate interface and of any photoelectrons from the Au substrate.[4,5,27] For the concentrated H_2O_2 photolysis experiments, a commercially available H_2O_2 solution (30%) was concentrated in a glass container by vacuum distillation, and the H_2O_2/H_2O vapor was deposited on ASW. The exposure of the codeposited H_2O_2/H_2O mixture on ASW was ~8 L at 90 K. For SO_2 photolysis experiments at 193 nm, prepared ASW was exposed to a mixture gas of $SO_2(5\%)+N_2(95\%)$ for 300 s, which resulted in net 8 L exposure of SO_2 on ASW. The surface of SO_2/water ice was kept refreshed by intermittent exposure of the SO_2 mixture gas to ASW during 193 nm photolysis experiments. In this experiment, a pulsed valve was opened after each laser shot so as to deposit a fresh layer of SO_2. The chamber pressure was 5×10^{-7} Torr during the intermittent deposition.

To photolyze water ice, unfocused 157 nm (or 193 nm) laser radiation was directed onto the ice surface at an angle of either ~80° or 45° to the surface normal. A suitable slit was used for the laser irradiation area to have the disk substrate with a radius of 6 mm. The incident fluence F was typically <0.1 mJ cm^{-2} $pulse^{-1}$ at 157 nm in 15 ns pulse duration. The F value at 193 nm was <1.0 mJ cm^{-2} $pulse^{-1}$. 193 nm irradiation of ASW produced no measurable REMPI signals of $O_2(X\ ^3\Sigma_g^-$ and $a\ ^1\Delta_g)$ and OH at such low incident intensities, although H atom photofragments from dimerlike water molecules on ASW surface were observed following 193 nm photodissociation of ASW.[28,29]

Photodesorbed $O_2(X\ ^3\Sigma_g^-)$ were ionized at a vertical distance of 2 mm from the ice surface by 2+1 REMPI process via the $C\ ^3\Pi_g(v'=2)\leftarrow X\ ^3\Sigma_g(v''=0)$ at 283–289 nm produced by frequency doubling the output of a Nd^{3+}:YAG (yttrium aluminum garnet) pumped dye laser (Lambda Physik, Göttingen, SCANmate),[30,31] and collected with a small mass spectrometer aligned perpendicular to the ice surface. Electronically excited $O_2(a\ ^1\Delta_g, v=0)$ photodesorbed from ASW has also been observed with the same experimental setup via the $d\ ^1\Pi_g(v'=1)\leftarrow a\ ^1\Delta_g(v''=0)$ REMPI transitions at 329–332 nm.[31,32] Johnson III *et al.*[31] suggested that the REMPI cross section for $O_2(a\ ^1\Delta_g)$ is at least an order of magnitude greater than that for $O_2(X\ ^3\Sigma_g^-)$. Photodesorbed $O(^3P_{J=2,1,0})$ atoms were ionized by the 2+1 REMPI transition via the $O(^3P_J-{}^3P_J)$ transition at 225.6–226.4 nm.[17] We tried to search for REMPI signals of oxygen molecules in the higher electronically excited states, i.e., $b\ ^1\Sigma_g^+$, $c\ ^1\Sigma_u^-$, and $^5\Pi_g$ using the REMPI transitions reported by Morrill *et al.*[32] and Slanger and Copeland,[33] but no evidence for these products was obtained.

III. SPECTRAL ANALYSIS

A. Simulation of 2+1 REMPI spectra of oxygen molecules

1. $O_2(X\ ^3\Sigma_g^-, v=0,1,2,3)$

The spectra were simulated using the program PGOPHER,[34] a program for simulating the rotational structure accompanying multiphoton electronic transitions. The simulated spectra were used to the estimate values of the rotational temperatures of the oxygen products. Spectroscopic parameters for the $X\ ^3\Sigma_g(v''=0,1)$ and $C\ ^3\Pi_g(v'=2)$ states of O_2 are summarized in Table I.[30,35–39] For spectral simulations of 2+1 REMPI via the sequence bands of the

$C\ ^3\Pi_g(v'=v''+2) \leftarrow X\ ^3\Sigma_g^-(v'')$ transitions for $v''=1$, 2, and 3, the literature constants for $C\ ^3\Pi_g(v'=2)$ and $X\ ^3\Sigma_g(v''=1)$ were adopted[35–39] since no information is available on the vibrationally excited levels. Although White and Beuhler[30] reported some assignments of the 2+1 REMPI spectrum via the $C\ ^3\Pi_g(v'=2) \leftarrow X\ ^3\Sigma_g(v''=0)$ transition, the Rydberg-valence state interactions with the repulsive $II\ ^3\Pi_g$ valence state resulted in highly perturbed rotational structures and large predissociation linewidths in the triplet manifold of the excited states. $O_2(X\ ^3\Sigma_g^-, v=0)$ via the spin forbidden REMPI $d\ ^1\Pi_g(v'=2) \leftarrow X\ ^3\Sigma_g^-(v''=0)$ transition was also included in the spectral simulation,[31,35] and the contribution to the observed $O_2(X\ ^3\Sigma_g^-, v=0)$ REMPI signals was found to be very small, less than 3%.

Rotational energy, E_{rot}, is characterized $\langle E_{rot}\rangle = k_B T_{rot}$, where k_B and T_{rot} are the Boltzmann constant and the rotational temperature, respectively.

2. $O_2(a\ ^1\Delta_g, v=0)$

Morrill *et al.*[32] reported the complex rotational structures in the REMPI spectra via the five $d\ ^1\Pi_g(v'=0-4)$ states due to the strong perturbations between $d\ ^1\Pi_g$ Rydberg and $II\ ^1\Pi_g$ valence states. The spectral segmenting is the result of avoided crossings between the rotational level manifolds of $d\ ^1\Pi_g(v'=1)$ and $II\ ^1\Pi_g(v'=5,6,7)$.[32] Unfortunately, we could not estimate the rotational temperature of the $O_2(a\ ^1\Delta_g, v=0)$ products because of these strong interactions.

B. Simulation of time-of-flight spectra of desorbed oxygen molecules

Time-of-flight (TOF) spectra of photoproducts were taken as a function of time, t, between the photolysis and REMPI laser pulses using a delay generator (Stanford Research) to investigate the translational energies of desorbing photoproducts. The measured TOF spectra, $S(t, T_{trans})$, were fitted to a sum of flux-weighted Maxwell–Boltzmann (MB) distributions, S_{MB}, with coefficients a_i, which are defined by a translational temperature, T_{trans}. Details regarding the simulation of such TOF spectra have been reported previously,[25]

$$S(t, T_{trans}) = \Sigma a_i S_{MB}(t, T_{trans}), \tag{8}$$

$$S_{MB}(t, T_{trans}) = r^3 t^{-4} \exp[-mr^2/2k_B T_{trans} t^2], \tag{9}$$

where r is the flight distance to the REMPI probe region. In these calculations we assume that signals come from a disk area (VUV photoirradiation area) with a radius of 6 mm. The MB distribution, $P_{MB}(E_{trans})$, as a function of translational energy, E_{trans}, is characterized by the averaged translational energy, $\langle E_{trans}\rangle = 2k_B T_{trans}$,[40]

$$P_{MB}(E_t) = (k_B T_{trans})^{-2} E_t \exp[-E_t/k_B T_{trans}]. \tag{10}$$

Conversion from the E_t distribution to the TOF distribution was performed using the Jacobian given by Zimmerman and Ho.[41] The angular distribution of the molecules photodesorbed from the ice surface was assumed to follow a $\cos^n\theta$ function, where θ is the surface polar coordinate. $n=0$ was adopted in the present best-fit procedures.[25,42]

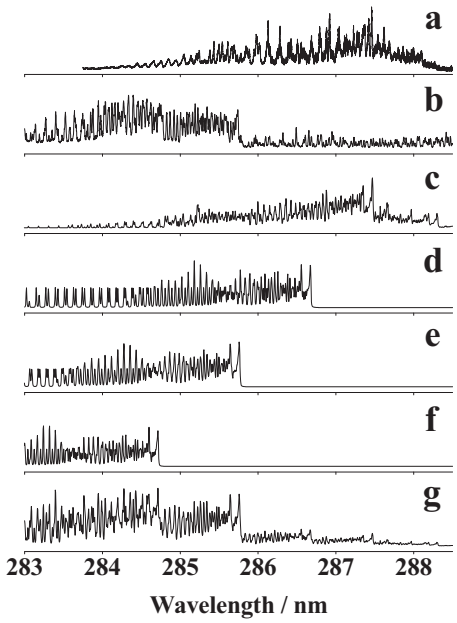

FIG. 1. 2+1 REMPI spectra of O_2 (a) following 157 nm photoirradiation of ASW. Time-of-flight is 1.5 μs; (b) following 193 nm photoirradiation of SO_2/ASW mixed ices. Time-of-flight is 1.5 μs. [(c)–(f)] Spectral simulation $C\ ^3\Pi_g(v'=v''+2) \leftarrow X\ ^3\Sigma_g^-(v'')$ transition, (c) $v''=0$ assuming a Boltzmann rotational state population distribution with $T_{rot}=2000$ K, and (d) $v''=1$, (e) $v''=2$, and (f) $v''=3$ assuming $T_{rot}=8000$ K. (g) Accumulated spectrum of (c), (d), (e), and (f) with the relative ratios of 0.05:0.2:1:1.

IV. RESULTS

A. Kinetic and rotational energy distributions of O_2 following 157 nm photodissociation of ASW

1. $O_2(X\ ^3\Sigma_g^-, v=0)$

Figure 1(a) shows a 2+1 REMPI spectrum following 157 nm photoirradiation of ASW at a fixed delay $t=1.5$ μs that corresponds to the peak TOF, as shown in Fig. 2. Highly perturbed rotational structures were observed in Fig. 1(a). By comparison with spectral simulation for $O_2(X\ ^3\Sigma_g^-, v=0)$ shown in Fig. 1(c), T_{rot} was estimated to be ~2000 K at $t=1.5$ μs. Figure 2 shows a typical TOF spectrum at 286.127 nm, which is characterized by $T_{trans}=4500\pm1000$ K and 500 ± 200 K. These results are summarized in Table II. Changing the REMPI probe wavelength to other wavelengths, no discernible change in the TOF profiles was ob-

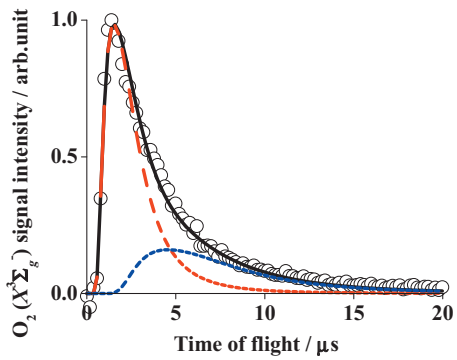

FIG. 2. Time-of-flight spectrum of $O_2(X\ ^3\Sigma_g^-, v=0)$ at a REMPI wavelength of 286.127 nm following 157 nm photoirradiation of ASW. The solid curves are fits to the data derived with $T_{trans}=4500$ and 500 K.

TABLE II. Translational and rotational temperatures of oxygen molecules following 157 nm photolysis of ASW and 193 nm photolysis of SO_2 on ASW at 90 K.

	Translational temperature T_{trans} (K)[a]	Averaged translational energy $\langle E_{trans}\rangle$ (kJ mol^{-1})	Rotational temperature T_{rot} (K)	Averaged rotational energy $\langle E_{rot}\rangle$ (kJ mol^{-1})	Reaction mechanism
$O_2(X\ ^3\Sigma_g^-, v=0)$ from ASW	4500 ± 1000(70%) 500 ± 200(30%)	75 ± 17 8 ± 3	~2000 [b] [d]	~17 [d]	$OH+O(^3P)$
$O_2(a\ ^1\Delta_g, v=0)$ from ASW	2500 ± 500 [c] 250 ± 100 [c]	42 ± 8 4 ± 2	[d]	[d]	$OH+O(^3P)$
$O_2(X\ ^3\Sigma_g^-, v=1-3)$ from SO_2 on ASW[e]	3000 ± 1000(55%) 500 ± 200(45%)	50 ± 17 8 ± 3	~8000 [b] [d]	~67 [d]	$O(^3P)+O(^3P)$

[a]Percentage in the parenthesis is a contributions of each temperature component.
[b]Measured at time-of-flight=1.5 μs.
[c]Each contribution depends on REMPI wavelength. See text for details.
[d]Not estimated. See text for details.
[e]With the relative ratios of 0.2: 1: 1 for $v=1:2:3$.

served. We were unable to estimate a rotational temperature for the $T_{trans}=500$ K component because of weak REMPI spectrum intensity.

2. $O_2(a\ ^1\Delta_g, v=0)$

Figures 3(a) and 3(b) show REMPI spectra following 157 nm photolysis of ASW, which were recorded at (a) $t=2.0$ μs and (b) 10.0 μs. Figure 4 shows TOF spectra at the two different REMPI wavelengths, (a) 329.965 nm for a high rotational level, and (b) 331.215 nm for a low rotational level. The TOF spectra are reproduced by two MB distributions with $T_{trans}=2500\pm500$ K and 250 ± 100 K with different contributions: (a) 80% and 20% at 329.965 nm and (b) 15% and 85% at 331.215 nm, respectively.

B. Evolution of O_2 signal intensity as a function of 157 nm photoirradiation time in the ASW photolysis

1. $O_2(X\ ^3\Sigma_g^-, v=0)$

The solid black line in Fig. 5(a) shows the time evolution of the $O_2(X\ ^3\Sigma_g^-, v=0)$ signal intensity at 286.127 nm recorded at $t=1.5$ μs as a function of 157 nm irradiation time on ASW. For comparison purpose, Fig. 5(a) includes the time evolution of photodesorbed $O(^3P_2)$ signal intensity that was recorded at the peak of TOF, i.e., $t=4.5$ μs.[17] The behaviors of $O_2(X\ ^3\Sigma_g^-, v=0)$ and $O(^3P_2)$ signals are in accordance to each other. Previously reported time evolution of the OH signal due to the H_2O_2 photoproduct on the 157 nm photoirradiated ASW surface was also included in Fig. 5(a), which reflects the concentration of photogenerated H_2O_2 on the ice surface.[15,43] The $O_2(X\ ^3\Sigma_g^-, v=0)$ REMPI signal increases faster than that of the H_2O_2 accumulated photolytically on the water ice surface.

2. $O_2(a\ ^1\Delta_g, v=0)$

Figures 5(b) and 5(c) show time evolution curves of $O_2(a\ ^1\Delta_g, v=0)$, which were recorded at (b) $t=2.0$ μs for $O_2(T_{trans}=2500$ K) at a high rotational level REMPI wavelength of 329.965 nm, and (c) $t=10.0$ μs for $O_2(T_{trans}=250$ K) at a low rotational level REMPI wavelength of 331.215 nm. Figures 5(b) and 5(c) also show the time evolution of the secondary photoproduct H_2O_2.[15,43] The curve for $O_2(T_{trans}=2500$ K) matches to that for H_2O_2. In addition, $O_2(T_{trans}=2500$ K) signals were observed promptly after 157 nm irradiation of H_2O_2/H_2O mixed ices, suggesting that the source of $O_2(T_{trans}=2500$ K) is photochemically produced H_2O_2 by 157 nm irradiation on ASW.

On the other hand, the $O_2(T_{trans}=250$ K) component appeared promptly upon 157 nm irradiation of ASW, as shown in Fig. 5(c). These results suggest that the source of the

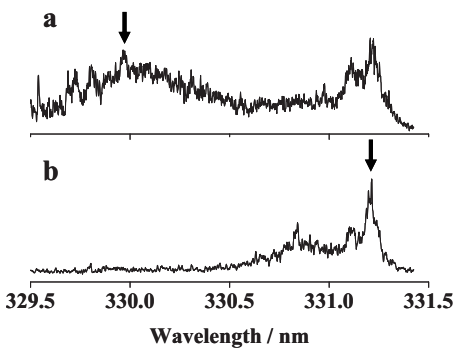

FIG. 3. (a) 2+1 REMPI spectrum of $O_2(a\ ^1\Delta_g, v=0)$ via the $d\ ^1\Pi_g(v'=1) \leftarrow a\ ^1\Delta_g(v''=0)$ transition following 157 nm photoirradiation of ASW. (a) $t=2.0$ μs and (b) $t=10.0$ μs. The arrows indicate the lines used when measuring the time-of-flight spectra.

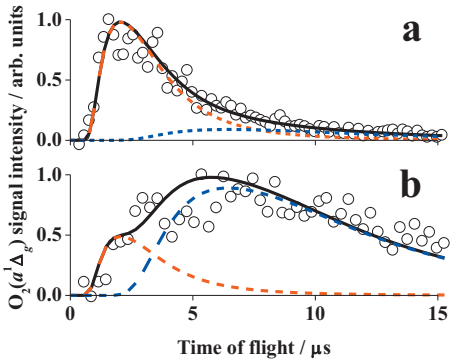

FIG. 4. Time-of-flight spectra of $O_2(a\ ^1\Delta_g, v=0)$ following 157 nm photoirradiation of ASW at (a) 329.965 nm and (b) 331.215 nm. The solid curves are fits to the data derived with $T_{trans}=2500$ and 250 K.

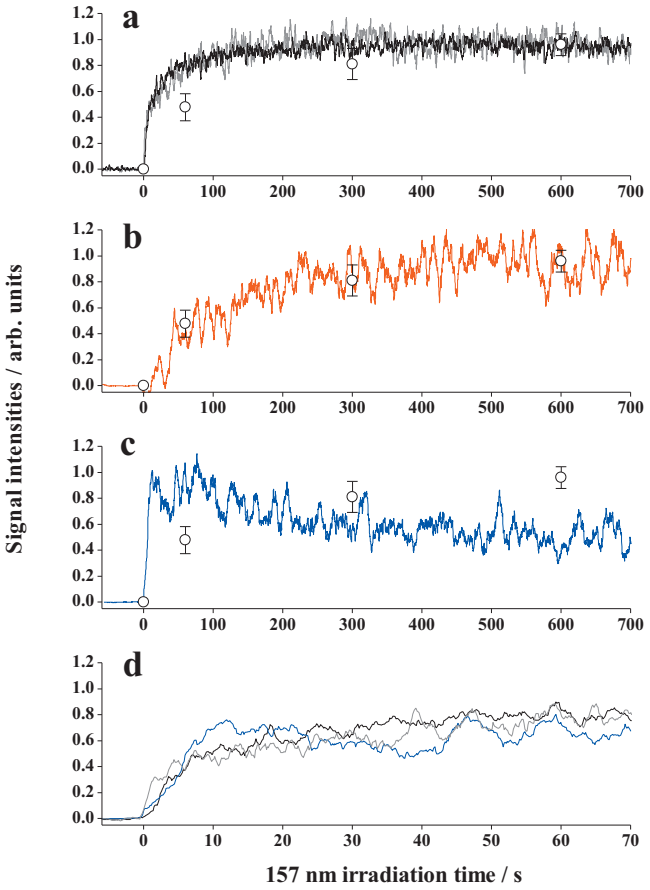

FIG. 5. (a) Time evolutions of $O_2(X\ ^3\Sigma_g^-, v=0)$ (black line) at $t=1.5$ μs at 286.127 nm and $O(^3P_2)$ (gray line) from ASW as a function of 157 nm irradiation time. The $O(^3P_2)$ signal was recorded at the peak time-of-flight of signal, $t=4.5$ μs. [(b) and (c)] Time evolutions of the $O_2(a\ ^1\Delta_g, v=0)$ at (b) $t=2.0$ μs (red line) at 329.965 nm and (c) $t=10.0$ μs (blue line) at 331.215 nm from ASW as a function of 157 nm irradiation time. Open circles in (a)–(c) represent the time evolution of H_2O_2 photoproducts accumulated on ASW (Refs. 15 and 43). (d) Expanded time evolution curves of the $O_2(X\ ^3\Sigma_g^-, v=0)$ (black line), $O_2(a\ ^1\Delta_g, v=0)$ (blue line), and $O(^3P_2)$ (gray line) signal intensity as a function of 157 nm irradiation time on ASW. The signal intensity of $O_2(a\ ^1\Delta_g, v=0)$ is adjusted for comparison.

$O_2(T_{trans}=250$ K) is different from that of the $O_2(T_{trans}=2500$ K). Figure 5(d) shows the expanded (<70 s) time evolution curves of $O_2(X\ ^3\Sigma_g^-, v=0)$, $O_2(a\ ^1\Delta_g, T_{trans}=250$ K), and $O(^3P_2)$. These three photoproducts were photodesorbed immediately after 157 nm irradiation started, and the time evolution behaviors are fairly similar to each other.

C. O_2 products following 193 nm photolysis of SO_2/H_2O mixed ice

193 nm irradiation of neat ASW produced no measurable REMPI signals of $O_2(X\ ^3\Sigma_g^-, v=0)$ and $O_2(a\ ^1\Delta_g, v=0)$. However, as SO_2 was deposited on ASW, $m/z=32$ signal was observed at 285.038 nm and its intensity increased, as shown in Fig. 6, i.e., O_2 was photodesorbed via reaction (7) following 193 nm photolysis of adsorbed SO_2 on ASW. Figure 1(b) shows a REMPI spectrum of O_2 following the 193 nm photoirradiation at $t=1.5$ μs that corresponds to the peak TOF of O_2 in Fig. 7. The TOF spectrum in Fig. 7 is characterized by $T_{trans}=3000\pm1000$ K and 500 ± 200 K. These results are summarized in Table II. $O_2(a\ ^1\Delta_g, v=0)$ failed to be detected at 329–332 nm.

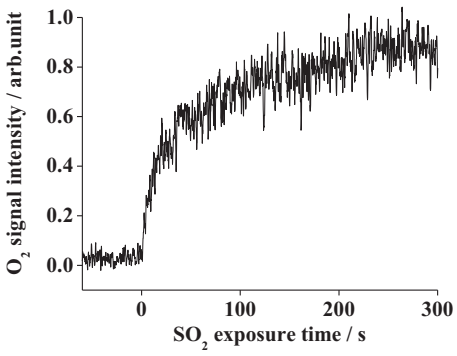

FIG. 6. Time evolution curve of the vibrationally excited $O_2(X\ ^3\Sigma_g^-)$ REMPI signal at 285.038 nm as a function of SO_2 exposure time at 157 nm at t $=1.5$ μs.

V. DISCUSSION

The 157 nm photolysis involves two primary processes; reactions (11) and (12),

$$H_2O(ads) + h\nu(157\ \text{nm}) \rightarrow H + OH(v=0\ \text{and}\ 1), \quad (11)$$

$$H_2O(ads) + h\nu(157\ \text{nm}) \rightarrow H_2 + O(^1D). \quad (12)$$

In the case of 157 nm photolysis ($E_{photon}=762$ kJ mol^{-1}), the available energies for reaction (11) is $E_{avail}(11)=220$ kJ mol^{-1} for OH($v=0$), and $E_{avail}(12)=38$ kJ mol^{-1}. $O(^1D)$ atoms via reaction (12) were successfully detected following 157 nm photolysis of ASW,[16] but would play only a minor role in the present study, considering the small quantum yields ($\leq$0.01 for 145–185 nm) in the gas phase,[10] and high reactivity of $O(^1D)$ with parent H_2O molecules by collisions with ASW to produce OH or H_2O_2.[44,45]

Our previous study showed that $O(^3P)$ atoms were photodesorbed immediately after 157 nm irradiation started, and are mainly formed by recombination of two OH radicals moving on the ASW surface, i.e., reaction (13),

$$OH + OH \rightarrow H_2O + O(^3P), \quad \Delta H = -67\ \text{kJ mol}^{-1}. \quad (13)$$

Considering reactions (11) and (13), we will discuss three possible O_2 desorption mechanisms; exothermic and endo-

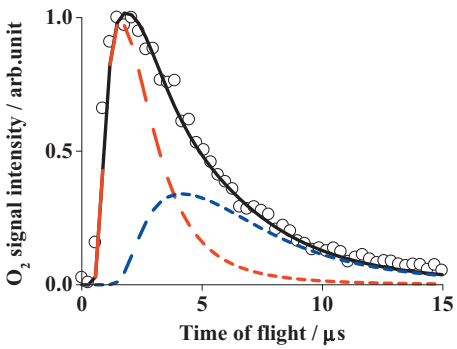

FIG. 7. Time-of-flight spectrum of O_2 following 193 nm photoirradiation of SO_2 adsorbed on ASW at 90 K at 285.038 nm. The solid curves are fits to the data with $T_{trans}=3000$ and 500 K.

thermic reactions of OH with $O(^3P)$, i.e., reactions (14) and (15), and two $O(^3P)$ recombination reaction, i.e., reaction (16),

$$\text{OH} + \text{O}(^3\text{P}) \rightarrow \text{O}_2\left(X\ ^3\Sigma_g^-\right) + \text{H}, \quad \Delta H = -68\ \text{kJ mol}^{-1}, \quad (14)$$

$$\text{OH} + \text{O}(^3\text{P}) \rightarrow \text{O}_2(a\ ^1\Delta_g) + \text{H}, \quad 26, \quad (15)$$

$$\text{O}(^3\text{P}) + \text{O}(^3\text{P}) + \text{M} \rightarrow \text{O}_2\left(X\ ^3\Sigma_g^-\right) + \text{M}, \quad -498. \quad (16)$$

A. $O_2(X\ ^3\Sigma_g^-, v=0)$ formation mechanisms

Figure 5(a) shows that the temporal signal behaviors of $O_2(X\ ^3\Sigma_g^-, v=0)$ and $O(^3P)$ are in fair agreement to each other, while OH signal intensity due to the H_2O_2 photoproducts on the 157 nm photoirradiated ASW surface increased slowly. These results indicate that $O_2(X\ ^3\Sigma_g^-, v=0)$ are not produced from the accumulated H_2O_2 photoproducts on the ASW surface.

On the assumptions that (a) a large amount of OH radicals are produced on the ASW surface after 157 nm laser shots on ASW, allowing successive surface reactions on the ASW surface to occur efficiently, and (b) the concentration of OH on ASW fed by primary photodissociation reaction (11) is much higher than that of $O(^3P)$ formed via secondary reaction (13), the appearance behavior of $O_2(X\ ^3\Sigma_g^-, v=0)$ signal intensity in Fig. 5(a) can be explained if the reaction schemes (17)–(21) proceeds on ASW,

$$\text{H}_2\text{O} + h\nu(157\ \text{nm}) \rightarrow \text{H} + \text{OH}(v = 0\ \text{and}\ 1), \quad (17)$$

$$\text{OH} + \text{OH} \rightarrow \text{H}_2\text{O}_2, \quad (18)$$

$$\text{OH} + \text{OH} \rightarrow \text{H}_2\text{O} + \text{O}(^3\text{P}), \quad (19)$$

$$\text{OH} + \text{O}(^3\text{P}) \rightarrow \text{O}_2\left(X\ ^3\Sigma_g^-, v = 0\right) + \text{H}, \quad (20)$$

$$\text{H}_2\text{O}_2 + h\nu(157\ \text{nm}) \rightarrow 2\text{OH}(v = 0\ \text{and}\ 1). \quad (21)$$

Furthermore, after successive 157 nm irradiation on ASW, OH radicals are accumulated on ASW since they can exist on/in water ice at 90 K.[3] These adsorbed OH on ASW can be additional sources for $O(^3P)$ via reactions (19) and (22),[17] and contribute to the $O_2(X\ ^3\Sigma_g^-, v=0)$ production, as shown in Fig. 5(a),

$$\text{OH(ads)} + h\nu(157\ \text{nm}) \rightarrow \text{H} + \text{O}(^3\text{P}), \quad E_{\text{avail}} = 278\ \text{kJ mol}^{-1}. \quad (22)$$

The translational temperature of $O_2(X\ ^3\Sigma_g^-, v=0)$ is much higher than the substrate temperature of 90 K, as shown in Table I. These results suggest that observed $O_2(X\ ^3\Sigma_g^-, v=0)$ originate only from the ASW surface, not from the bulk. Kimmel and their co-workers[4,5] suggested that O_2 formation occurred at or near the ASW/vacuum interface in the low-energy electron-stimulated desorption experiments. The electron-stimulated migration of OH or OH^- to the vacuum interface, where they react and produce O_2, occurs via transport through the hydrogen bond network of the ASW.[4,5]

Arasa *et al.* performed molecular dynamics simulations of the UV photodissociation of ASW at 10–90 K. They reported that OH desorbs into the vacuum only when they were generated from the top 3 ML of ASW at 90 K and its probability is <0.05 per adsorbed UV photon, whereas most of OH are trapped on/in ASW.[46] Andersson *et al.*[47,48] predicted that OH radicals in bulk ASW formed following photodissociation of ASW move only less than 0.5 nm, while OH radicals formed in the top 3 ML of ASW were able to move up to more than 6 nm until they were trapped. This large mobility of OH on the top ASW makes secondary reactions of OH with adsorbed species possible. These models support our proposed reaction schemes.

B. $O_2(a\ ^1\Delta_g, v=0)$ formation mechanisms

The time evolution curve for $O_2(a\ ^1\Delta_g, T_{\text{trans}}=250\ \text{K})$ recorded at $t=10.0\ \mu\text{s}$ appears promptly, as shown in Fig. 5(c). Furthermore, Fig. 5(d) shows that $O_2(a\ ^1\Delta_g, v=0)$, $O(^3P_2)$, and $O_2(X\ ^3\Sigma_g^-, v=0)$ were photodesorbed immediately after the 157 nm irradiation started. Since vibrationally excited $OH(v=1)$ are produced from primary photodissociation of H_2O,[15] $O_2(a\ ^1\Delta_g, T_{\text{trans}}=250\ \text{K})$ can be produced via reaction of vibrationally excited $OH(v=1)$ and $O(^3P)$, as Lunt *et al.* observed in the gas phase, i.e., reaction (23),[23]

$$\text{OH}(v = 1) + \text{O}(^3\text{P}) \rightarrow \text{O}_2(a\ ^1\Delta_g, v = 0) + \text{H}, \quad \Delta H = -17\ \text{kJ mol}^{-1}. \quad (23)$$

On the other hand, Fig. 5(b) shows that $O_2(a\ ^1\Delta_g, T_{\text{trans}}=2500\ \text{K})$ was not observed immediately after 157 nm photoirrradiation, and the appearance behavior is in accordance with the concentration of photogenerated H_2O_2 on the ice surface. Furthermore, the $O_2(a\ ^1\Delta_g, T_{\text{trans}}=2500\ \text{K})$ was observed promptly after 157 nm irradiation of the H_2O_2/H_2O mixed ices. These results suggest that H_2O_2 photoproduct on ASW is a source for the $O_2(a\ ^1\Delta_g, T_{\text{trans}}=2500\ \text{K})$ formation. Hama *et al.*[15] previously reported that $OH(v=0\ \text{and}\ 1, T_{\text{trans}}=7500\ \text{K})$ are produced from the secondary photodissociation of H_2O_2 that is photolytically accumulated on the ASW surface by 157 nm irradiation, i.e., reaction (24),

$$\text{H}_2\text{O}_2(\text{ads}) + h\nu(157\ \text{nm}) \rightarrow 2\text{OH}(v = 0\ \text{and}\ 1, T_{\text{trans}} = 7500\ \text{K}), \quad (24)$$

where $E_{\text{avail}}(24)$ is $493\ \text{kJ mol}^{-1}$. These $OH(v=0\ \text{and}\ 1, T_{\text{trans}}=7500\ \text{K})$ can proceed in endothermic reactions on ASW surface.[16] Thus, $O_2(a\ ^1\Delta_g, T_{\text{trans}}=2500\ \text{K})$ can be produced from the hot photoproducts such as OH from H_2O_2 via reaction (25),

$$\text{OH}(v = 0\ \text{and}\ 1, T_{\text{trans}} = 7500\ \text{K}) + \text{O}(^3\text{P}) \rightarrow \text{O}_2(a\ ^1\Delta_g, T_{\text{trans}} = 2500\ \text{K}) + \text{H}. \quad (25)$$

Lunt *et al.*[23] reported 0.025 for the yield of $O_2(a\ ^1\Delta_g)$ formation via reaction of $OH(v \geq 1)$ with $O(^3P)$ in the gas phase, and the majority of the products are $O_2(X\ ^3\Sigma_g^-)$. Lique *et al.*[21] pointed out a possibility of the nonadiabatic transition for the OH+O reaction. The potential energy surface of OH+O reaction corresponding to the electronically excited $2A'$ state correlates only with the $O_2(a\ ^1\Delta_g)$+H product channel through the electronically excited state of the

$HO_2(2A')$ complex, but nonadiabatic electronic relaxation of this complex to the lowest $2A''$ state can provide $O_2(X\ ^3\Sigma_g^-)$ +H product channel.[21] Our previous observations of vibrational distribution of $OH(v=1/v=0)$ produced via reactions (17) and (24) were both 0.2 ± 0.1.[15] These previously reported results suggest that the relative product ratio of $O_2(a\ ^1\Delta_g, v=0)$ would be small in the present study.

C. Other possible O_2 formation mechanisms

To consider a contribution of highly exothermic recombination reaction of two $O(^3P)$, we measured the translational and internal energy distributions of O_2 following 193 nm photoexcitation of SO_2 adsorbed on ASW since $O(^3P)$ were efficiently produced from the 193 nm photolysis of SO_2.[49] As shown in Figs. 1(b), 6, and 7, 193 nm photolysis of SO_2 on ASW yielded O_2 products via subsequent reactions (26) and (27) and they were desorbed into the vacuum,

$$SO_2(\text{ads}) + h\nu(193\ \text{nm}) \rightarrow SO + O(^3P), \quad E_{\text{avail}}\ (\text{kJ mol}^{-1}):\ 43 \qquad (26)$$

$$O(^3P) + O(^3P) + M \rightarrow O_2(X\ ^3\Sigma_g^-) + M, \quad \Delta H\ (\text{kJ mol}^{-1}):\ -498. \qquad (27)$$

The available energy for reaction (26) at 193 nm (E_{photon} =620 kJ mol^{-1}) was calculated using dilute solution phase thermodynamic data for the adsorbed SO_2(ads).[20] The REMPI spectrum of Fig. 1(b) may be simulated by a sum of the sequence bands of the $C\ ^3\Pi_g(v'=v''+2) \leftarrow X\ ^3\Sigma_g(v'')$ transitions mainly for $v''=2$ and 3 [Fig. 1(g)]. In addition, $O_2(a\ ^1\Delta_g, v=0)$ was failed to be detected at 329–332 nm. These results indicate that highly exothermic reaction (27) yields mainly vibrationally excited $O_2(X\ ^3\Sigma_g^-, v=2$ and 3), and plays only a minor role in the formation of $O_2(X\ ^3\Sigma_g^-, v=0)$ and $O_2(a\ ^1\Delta_g, v=0)$ from neat ASW photolysis at 157 nm.

Hydroperoxyl radical, HO_2, is known to be photodissociated to OH and $O(^1D$ or $^3P)$ at excitation wavelengths of 248–147 nm in the gas phase.[50–52] Our previous studies showed no contribution of HO_2 photoproducts on ASW to production of OH and $O(^1D$ and $^3P)$ following 157 nm photolysis of ASW, suggesting that the amount of HO_2 photoproducts on the ice surface was negligible at 90 K. Therefore, the O_2 formation following reactions of HO_2+H or HO_2+OH are considered to be unlikely sources for the observed O_2 ejection from the ASW surface in the present experiments.[3,53,54] Theoretical and experimental studies reported that the probabilities for the photodissociation processes of HO_2 to H+O_2 fragments were estimated to be small, since this photoprocesses are prohibited by potential barriers.[52,55]

VI. CONCLUSION

We have measured time-of-flight and rotational spectra of the photodesorbed $O_2(X\ ^3\Sigma_g^-, v=0)$ and $O_2(a\ ^1\Delta_g, v=0)$ following pulsed 157 nm irradiation of ASW at 90 K, and the translational and internal energy distributions were obtained. Measured translational energies of $O_2(X\ ^3\Sigma_g^-, v=0)$ and $O_2(a\ ^1\Delta_g, v=0)$ suggested that the observed $O_2(X\ ^3\Sigma_g^-, v=0)$ and $O_2(a\ ^1\Delta_g, v=0)$ fragments originate only from the ASW surface, not from the ice bulk. The exothermic barrierless reaction of OH and $O(^3P)$ is proposed as the most plausible source for $O_2(X\ ^3\Sigma_g^-, v=0)$ formation. The reaction of translationally and internally excited OH with $O(^3P)$ plays a key role in the $O_2(a\ ^1\Delta_g, v=0)$ formation. The contribution of recombination reaction of two $O(^3P)$ to O_2 formation was found to be negligible. $O(^3P)$ would react with OH much more frequently than they encounter another $O(^3P)$ to produce O_2 since concentration of primary product OH on ASW is much higher than that of $O(^3P)$ formed via secondary reaction on ASW.

ACKNOWLEDGMENTS

This work was supported by a Grant-in-Aid from the JSPS (Grant No. 20245005). The authors thank Dr. R. Wada of Nagoya University for useful suggestions in simulation of the rotational spectra of the O_2 molecules.

[1] E. L. Gibb, D. C. B. Whittet, A. C. A. Boogert, and A. G. G. M. Tielens, Astrophys. J., Suppl. Ser. **151**, 35 (2004).
[2] J. K. Davies, T. L. Roush, D. P. Cruikshank, M. J. Bartholomew, T. R. Geballe, T. Owen, and C. de Bergh, Icarus **127**, 238 (1997).
[3] C. Laffon, S. Lacombe, F. Bournel, and Ph. Parent, J. Chem. Phys. **125**, 204714 (2006).
[4] N. G. Petrik, A. G. Kavetsky, and G. A. Kimmel, J. Phys. Chem. B **110**, 2723 (2006).
[5] N. G. Petrik, A. G. Kavetsky, and G. A. Kimmel, J. Chem. Phys. **125**, 124702 (2006).
[6] C. T. Reimann, J. W. Boring, R. E. Johnson, J. W. Garrett, K. R. Farmer, W. L. Brown, K. J. Marcantonio, and W. M. Augustyniak, Surf. Sci. **147**, 227 (1984).
[7] M. S. Westley, R. A. Baragiola, R. E. Johnson, and G. A. Baratta, Nature (London) **373**, 405 (1995).
[8] M. S. Westley, R. A. Baragiola, R. E. Johnson, and G. A. Baratta, Planet. Space Sci. **43**, 1311 (1995).
[9] K. I. Öberg, H. Linnartz, R. Visser, and E. F. van Dishoeck, Astrophys. J. **693**, 1209 (2009).
[10] L. J. Stief, W. A. Payne, and R. B. Klemm, J. Chem. Phys. **62**, 4000 (1975).
[11] D. H. Mordaunt, M. N. R. Ashfold, and R. N. Dixon, J. Chem. Phys. **100**, 7360 (1994).
[12] S. A. Harich, X. Yang, D. W. H. Hwang, J. J. Lin, X. Yang, and R. N. Dixon, J. Chem. Phys. **114**, 7830 (2001).
[13] A. Y.-M. Ung, Chem. Phys. Lett. **28**, 603 (1974).
[14] M. Seki, K. Kobayashi, and J. Nakahara, J. Phys. Soc. Jpn. **50**, 2643 (1981).
[15] T. Hama, A. Yabushita, M. Yokoyama, M. Kawasaki, and S. Andersson, J. Chem. Phys. **131**, 054508 (2009).
[16] T. Hama, A. Yabushita, M. Yokoyama, M. Kawasaki, and N. Watanabe, J. Chem. Phys. **131**, 114510 (2009).
[17] T. Hama, A. Yabushita, M. Yokoyama, M. Kawasaki, and N. Watanabe, J. Chem. Phys. **131**, 114511 (2009).
[18] S. P. Sander, B. J. Finlayson-Pitts, R. R. Friedl, D. M. Golden, R. E. Huie, H. Keller-Rudek, C. E. Kolb, M. J. Kurylo, M. J. Molina, G. K. Moortgat, V. L. Orkin, A. R. Ravishankara, and P. H. Wine, JPL Publication 06-2, Jet Propulsion Laboratory, Pasadena, 2006.
[19] A. J. Matich, M. G. Bakker, D. Lennon, T. I. Quickenden, and C. G. Freeman, J. Chem. Phys. **97**, 10539 (1993).
[20] M. K. Karapet'yants and M. K. Karapet'yants, *Handbook of Thermodynamic Constants of Inorganic and Organic Compounds* (Ann Arbor-Humphrey Science, London, 1970).
[21] F. Lique, M. Jorfi, P. Honvault, P. Halvick, S. Y. Lin, H. Guo, D. Q. Xie, P. J. Dagdigian, J. Kłos, and M. H. Alexander, J. Chem. Phys. **131**, 221104 (2009).
[22] J. A. Dodd, S. J. Lipson, and W. A. M. Blumberg, J. Chem. Phys. **92**, 3387 (1990).
[23] S. T. Lunt, G. Marston, and R. P. Wayne, J. Chem. Soc., Faraday Trans.

2 **84**, 899 (1988).
[24] W. Zheng, D. Jewitt, and R. I. Kaiser, Chem. Phys. Lett. **289**, 435 (2007).
[25] A. Yabushita, Y. Inoue, T. Senga, M. Kawasaki, and S. Sato, J. Phys. Chem. B **106**, 3151 (2002).
[26] S. Sato, D. Yamaguchi, K. Nakagawa, Y. Inoue, A. Yabushita, and M. Kawasaki, Langmuir **16**, 9533 (2000).
[27] N. G. Petrik and G. A. Kimmel, J. Phys. Chem. C **113**, 4451 (2009).
[28] A. Yabushita, Y. Hashikawa, A. Ikeda, M. Kawasaki, and H. Tachikawa, J. Chem. Phys. **120**, 5463 (2004).
[29] A. Yabushita, D. Kanda, N. Kawanaka, M. Kawasaki, and M. N. R. Ashfold, J. Chem. Phys. **125**, 133406 (2006).
[30] M. G. White and R. J. Beuhler, J. Chem. Phys. **120**, 2445 (2004).
[31] R. D. Johnson III, G. R. Long, and J. W. Hudgens, J. Chem. Phys. **87**, 1977 (1987).
[32] J. S. Morrill, M. L. Ginter, E. S. Hwang, T. G. Slanger, R. A. Copeland, B. R. Lewis, and S. T. Gibson, J. Mol. Spectrosc. **219**, 200 (2003).
[33] T. G. Slanger and R. A. Copeland, Chem. Rev. (Washington, D.C.) **103**, 4731 (2003) (and references therein).
[34] C. M. Western, PGOPHER, a program for simulating rotational structure, University of Bristol, available at http://pgopher.chm.bris.ac.uk.
[35] J. S. Morrill, M. L. Ginter, S. T. Gmibson, and B. R. Lewis, J. Chem. Phys. **111**, 173 (1999).
[36] C. Coletti and G. D. Billing, Chem. Phys. Lett. **356**, 14 (2002).
[37] G. Herzberg, *Spectra of Diatomic Molecules* (Van Nostrand, Princeton, NJ, 1950).
[38] D. L. Albritton, W. J. Harrop, A. L. Schmeltekopf, and R. N. Zare, J. Mol. Spectrosc. **46**, 103 (1973).
[39] J. W. C. Johns and D. W. Lepard, J. Mol. Spectrosc. **55**, 374 (1975).
[40] F. M. Zimmermann and W. Ho, J. Chem. Phys. **100**, 7700 (1994).
[41] F. M. Zimmermann and W. Ho, Surf. Sci. Rep. **22**, 127 (1995).
[42] A. Yabushita, Y. Inoue, T. Senga, M. Kawasaki, and S. Sato, J. Phys. Chem. A **108**, 438 (2004).
[43] A. Yabushita, T. Hama, D. Iida, and M. Kawasaki, J. Chem. Phys. **129**, 014709 (2008).
[44] E. J. Dunlea and A. R. Ravishankara, Phys. Chem. Chem. Phys. **6**, 3333 (2004).
[45] W. Zheng, D. Jewitt, and R. I. Kaiser, Phys. Chem. Chem. Phys. **9**, 2556 (2007).
[46] C. Arasa, S. Andersson, H. M. Cuppen, E. F. van Dishoeck, and G.-J. Kroes, J. Chem. Phys. **132**, 184510 (2010).
[47] S. Andersson, A. Al-Halabi, G.-J. Kroes, and E. F. van Dishoeck, J. Chem. Phys. **124**, 064715 (2006).
[48] S. Andersson and E. F. van Dishoeck, Astron. Astrophys. **491**, 907 (2008).
[49] M. Brouard, R. Cireasa, A. P. Clark, T. J. Preston, C. Vallance, G. C. Groenenboom, and O. S. Vasyutinskii, J. Phys. Chem. A **108**, 7965 (2004).
[50] L. C. Lee, J. Chem. Phys. **76**, 4909 (1982).
[51] A. Sinha, J. Coleman, and R. Barnes, J. Phys. Chem. **98**, 12462 (1994).
[52] M. Suto and L. C. Lee, J. Chem. Phys. **80**, 195 (1984).
[53] S. H. Mousavipour and V. Saheb, Bull. Chem. Soc. Jpn. **80**, 1901 (2007).
[54] S. H. Mousavipour and I. Yousefiasl, Bull. Chem. Soc. Jpn. **82**, 953 (2009).
[55] S. R. Langhoff and R. L. Jaffe, J. Chem. Phys. **71**, 1475 (1979).